EEG-Based Continuous Hand Movement Decoding Using Improved Center-Out Paradigm

Jiarong Wang, Luzheng Bi, *Senior Member, IEEE*, Weijie Fei, and Kun Tian

***Abstract*— The continuous decoding of human movement intention based on electroencephalogram (EEG) signals is valuable for developing a more natural motor augmented or assistive system instead of its discrete classifications. The classic center-out paradigm has been widely used to study discrete and continuous hand movement parameter decoding. However, when applying it in studying continuous movement decoding, the classic paradigm needs to be improved to increase the decoding performance, especially generalization performance. In this paper, we first discuss the limitations of the classic center-out paradigm in exploring the hand movement's continuous decoding. Then, an improved paradigm is proposed to enhance the continuous decoding performance. Besides, an adaptive decoder-ensemble framework is developed for continuous kinematic parameter decoding. Finally, with the improved center-out paradigm and the ensemble decoding framework, the average Pearson's correlation coefficients between the predicted and recorded movement kinematic parameters improve significantly by about 75 percent for the directional parameters and about 10 percent for the non-directional parameters. Furthermore, its generalization performance improves significantly by about 20 percent for the directional parameters. This study indicates the advantage of the improved paradigm in predicting the hand movement's kinematic information from low-frequency scalp EEG signals. It can advance the applications of the noninvasive motor brain-computer interface (BCI) in rehabilitation, daily assistance, and human augmentation areas.**

***Index Terms*— Electroencephalogram, brain-computer interface, hand movement, continuous decoding.**

I. Introduction

BRAIN-COMPUTER interface (BCI) is of utmost value because it can translate human mind from neural signals to control devices directly without activating peripheral nerve or muscles [1]. Brain signals can be recorded invasively or non-invasively [2]. Considering the advantages of low-cost, portability, less trauma, and not relying on medical and surgical expertise, in the present work, we concentrate on the non-invasive electroencephalogram (EEG) recording way [3].

Upon past decades, EEG-based BCIs have progressed greatly covering application fields of communication [1], teleoperation [4], rehabilitation [5], daily life assistance [6], entertainment [7], and so on. Among various kinds of BCIs, motor-BCIs can detect brain oscillations associated with imagined, or executed, or attempted movements [8]. Thus, motor-BCIs are valuable to be applied in combination with neuroprosthetic devices, exoskeletons or robotic arms to assist, restore and augment impaired motor abilities of patients [9], [10]. Besides, motor-BCIs are also valuable for the healthy people to develop an active human-machine interaction system by decoding human movement intention [11], [12]. Compared with motor imagery paradigms which induce EEG modalities by imagining movements repetitively, detecting and recognizing movement intentions utilizing residual or intact movement functions are more intuitive and natural.

It is known that human movement intentions are encoded in movement-related cortical potentials (MRCPs), which can be captured from low-frequency scalp EEG signals [13]. Over past decades, numerous studies were dedicated to investigating the neural correlates and decoding of hand movement intention based on MRCPs. From neurophysiological aspect, several studies tried to uncover the brain activity and neural response associated with hand movement, and showed that the primary sensorimotor cortex and the mesial premotor areas were activated during the hand movement, and movement-related regional activation was predominant over the contralateral premotor and primary sensorimotor cortex [14], [15]. From decoding aspect, kinetic and kinematics movement parameters, including force/torque [16], velocity/speed [17], trajectory/distance [18], [19] and direction [20], were explored to be decoded from MRCPs. Besides, hand movement types extracted from actual application scenarios were also decoded in [21] and movement onset were detected in [22]. In further, studies [13], [22] exhibited the relation between the MRCPs and movement parameters, and results in [13] indicated that the magnitude and time course of bereitschaftspotential (BP) can be influenced by various movement factors such as movement torque-level, speed, precision and complexity.

Manuscript received 6 July 2022; revised 2 September 2022; accepted 28 September 2022. Date of publication 3 October 2022; date of current version 20 October 2022. This work was supported by the National Natural Science Foundation of China under Grant 51975052. *(Corresponding authors: Weijie Fei; Kun Tian.)*

This work involved human subjects or animals in its research. Approval of all ethical and experimental procedures and protocols was granted by the Ethics Committee of Beijing Institute of Technology and performed in line with the Declaration of Helsinki.

Jiarong Wang, Luzheng Bi, and Weijie Fei are with the School of Mechanical Engineering, Beijing Institute of Technology, Beijing 100081, China (e-mail: 18810805389@163.com; bhxblz@bit.edu.cn; 3120170241@bit.edu.cn).

Kun Tian is with Beijing Huawei Digital Technologies Company Ltd., Beijing 100095, China (e-mail: kun.tian@huawei.com).

This article has supplementary downloadable material available at https://doi.org/10.1109/TNSRE.2022.3211276, provided by the authors.

Digital Object Identifier 10.1109/TNSRE.2022.3211276

These studies showed the possibility of decoding hand movement parameters from the low-frequency EEG signals and correlated the physical hand movement with neural activity.

To sum up, for the hand movement parameters decoding, it could be divided into two categories: discrete classification (e.g., the movement directions/ types discrimination or movement onset detection) and continuous regression (e.g., the movement velocity/ trajectory reconstruction). For the hand movement classification, the classic center-out paradigm was used by various studies due to its fundamentality and generalizability. Chouhan et al. [23] investigated the upper limb movement directions decoding using the classic center-out paradigm, and proposed a wavelet phase-locking value-based method which achieved a mean binary classification accuracy of 76.85%. Similar work was done in [24], and Robinson et al. proposed a novel signal processing technique to extract features from EEG signals, and the classification accuracy of four-class center-out movement directions was $80.24 \pm 9.41\%$. Besides, in [17], Robinson et al. designed an experiment in which the subjects were required to perform the center-out right-hand movement at two speed levels, and they used the Wavelet-Common Spatial Pattern algorithm to classify the movement speed, which yielded a mean accuracy of 83.71%. Considering that, in practice, people are often distracted by other tasks or environmental factors, Bi et al. [25] first proposed a hierarchical decoding model based on attention state estimation to decode the hand movement onset intention in the right-hand center-out paradigm. In [26], Fei et al. explored to the robust decoding of movement directions to the cognitive distraction in the center-out paradigm by using the Riemannian Manifold-based method, and the simulation and experimental results showed that the Riemannian-based methods have higher robustness to cognitive distraction. When exploring the continuous movement decoding issues, several studies followed the center-out paradigm. In these studies, hand movement kinematic components projected onto the x and y axes were decoded from low-frequency EEG signals. In [27], Bradberry et al. explored the ability to continuously decode 3D hand velocity from EEG signals during natural, center-out reaching movements. In [28], Robinson et al. adopted the center-out paradigm and estimated movement trajectory using a Kalman filter model with informative predictors subset selection, and finally the correlation between recorded and estimated data achieved 0.57 ± 0.07. In [29], Jeong et al. involved the center-out right-handed reaching movement in 3D space and proposed a multi-directional deep learning framework. Finally, the decoding performances for six directions in 3D space reached the grand-averaged correlation coefficients of 0.47 and the normalized root mean square error below 0.2. Besides, in [30], úbeda et al. used a multidimensional linear regression to decode upper limb kinematics from EEG signals in center-out reaching tasks and then classified the reaching targets with the 8-class classification accuracy of 29%. In [31], Lv et al. reconstructed the hand movement velocity using EEG signals recorded during a self-routed drawing task, which was improved from center-out reaching task, and the average correlation coefficients between the measured and the decoded velocities are 0.37 for the horizontal dimension and 0.24 for the vertical dimension.

Though numerous studies have explored the EEG-based continuous decoding of hand/ upper limb movement using the center-out paradigm as mentioned above, there is a common issue in these studies, which could deteriorate the decoding performance. It was that, in the classic center-out paradigm, the hand movement in each trial was either along the X-axis directions or the Y-axis directions. In this case, the projected component of each point-to-point movement was mostly centralized on one axis and was near zero on another axis. In fact, to decode kinematic parameters, we have to build regression models between kinematic parameters (dependent variables) and EEG signals (independent variables). However, for the classic center-out paradigm, trials associated with two directions (left and right directions) on the X axis do not generate training data for decoding v_y/p_y. Likewise, trials on the Y axis do not generate training data for decoding v_x/p_x. It means that only half of all trials contribute to building each kinematic parameter decoding model. Furthermore, to guarantee the generalization of the decoding model in the whole 2-D plane, the more general scenarios (i.e., both v_x/p_x and v_y/p_y are not equal to zero) need to be provided. In addition to the mentioned-above disadvantages, other disadvantages of the classic center-out paradigm, e.g., shorter upper limb movement range, could limit its effectiveness in hand movement decoding.

To address these weaknesses of the classic center-out paradigm, in this study, we proposed an improved center-out paradigm, where the subjects were required to move their hands in four orthogonal directions at an angle of 45° from the cartesian coordinate axes, and developed an adaptive decoder-ensemble framework for the continuous hand movement decoding.

The contribution of this paper is that it is the first work to explore how to increase the decoding performance, especially generalization performance when predicting/ reconstructing hand movement parameters from EEG signals by improving the center-out paradigm. Specially, we design a new center-out paradigm, and experimental results show that the new paradigm has advantages in improving decoding performance and generalization performance in the whole 2-D plane. Our work can promote the application of the EEG-based motor-BCIs for rehabilitation, assistance, and human augmentation.

II. Experiment and Methods

A. Participants and Equipment

The experiment was conducted at the IHMS laboratory, Beijing Institute of Technology, Beijing, China. Eight subjects (right-handed, aged from 22 to 26 at the measurement time) were recruited to participate our experiment. All of them confirmed having no brain disease and the vison was corrected to be normal. Before formal experiments, all subjects were informed of experimental purpose and requirements, and sighed the consent to participate in the experiment. The experimental procedure adhered to the Declaration of Helsinki and was approved by the ethics committee of Beijing Institute

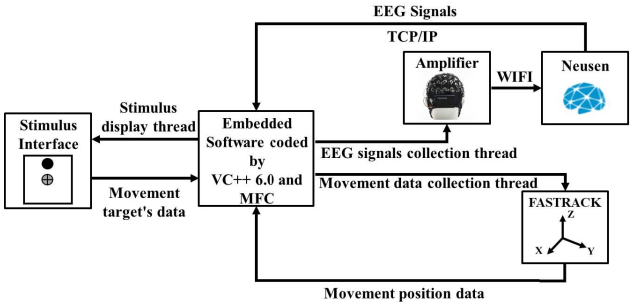

Fig. 1. The schematic diagram of the experiment system. The system is coded based on VC++ 6.0 and MFC application framework and implements data collection, data alignment and experimental stimulus interface display.

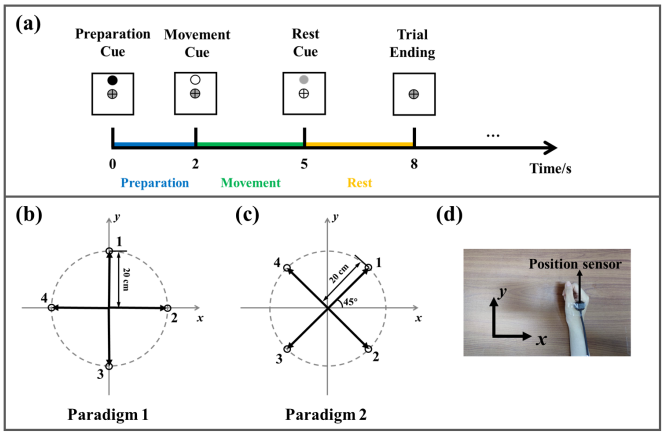

Fig. 2. The experimental timeline and setup. (a) The experimental timeline of one trial. (b) and (c) illustrate the hand movement directions of Paradigms 1 and 2 in the coordination system, respectively. 1, 2, 3, and 4 correspond to four movement directions. (d) Real experimental scene of hand movement and its corresponding coordination system.

of Technology. The number of subjects was evaluated by the Power tables from *Cohen* [32] to justify that the number of subjects involved in our experiment was sufficient for statistical test. The effect size of F-ratios was calculated by Equation (1), as follows:

$$f^2 = \frac{R^2}{1 - R^2}, \tag{1}$$

where R^2 is the partial eta squared value and was calculated as 0.414 by ANOVA in IBM SPSS Statistics 25, and then f^2 is calculated as 0.7065. According to the Power tables, when f^2 is 0.7065, the equivalent effect size d is 1.7. The calculation of the number of subjects needed to obtain a significant result was done in G* Power version 1.1.9.7 [33]. When selecting Wilcoxon signed-rank test for statistical test, with the given two-tailed $\alpha = 0.05$ and the recommended power level of 80%, the recommended number of subjects was 6, which justified the sufficiency of subjects in our experiment.

A NeuSen.W64 Neuracle 64-channel EEG amplifier was used for EEG signals recording. The sampling rate of the amplifier was set to be 1000 Hz. A FASETRACK position sensor was used to collect the hand movement positions. The sampling rate of the sensor was 60 Hz. The data collection, data alignment and experimental stimulus interface display were accomplished by the system coded by us based on the software VC++ 6.0 and Microsoft Foundation Classes application framework, as shown in Fig. 1.

B. Experimental Paradigms

This study involved two experimental paradigms, i.e., the classic center-out paradigm, namely as Paradigm 1, and the improved center-out paradigm, namely as Paradigm 2. The hand movement tasks involved in this study were in horizontal 2D plane. There were four movement targets in both paradigms, namely as 1, 2, 3, and 4. The illustration of hand movement directions of two paradigms was shown in Fig. 2 (b) and (c). For the Paradigm 1, the four movement targets were located at the four axes of cartesian coordinate and the starting paradigm 2, the four movement targets were located at four straights who were at an angle of 45° from the cartesian coordinate axes and the starting point of movement was also the origin of the coordinate. The movement range for each target in both paradigms was 20 cm. The projection scale between the cursor movement distance on the screen and the real hand movement distance was 1.5:1.

The timeline for each experiment trial is shown in Fig. 2(a). Each experimental trial contained three periods: preparation period (2 s), movement period (3 s), rest period (3 s). The circle with a cross in the center position corresponded to the home position. The gray solid circle corresponded to the cursor to be moved by the subjects, and its positions were the real-time positions of sensor. At the beginning of each experimental block, the real-time hand position was re-aligned to be the home position. At the 0 s, one trial started, and the black solid circle appeared in one of four target positions randomly as the target cue. At the 2 s, the black solid circle of the target cue changed into the hollow circle as the movement cue, and when it occurred, the subjects were asked to move their hands from the home position to the target position immediately. At the 5 s, the hollow circle of the target position disappeared, indicating the subjects moved the hands back to the initial home position. At the 8 s, one trial ended.

For each paradigm, there were 15 blocks, and each block consisted of 16 trials. For each block, four movement targets were shown randomly with equal appearance times (4 times for each target). It meant that we would obtain 240 trials in all for each paradigm. Two paradigms' blocks were alternately conducted for experimental order-balance.

C. Data Acquisition

EEG data was recorded from 61 active electrodes according to the international 10-20 system, with the forehead ground electrode positioned at AFz and the reference electrode positioned at CPz. The locations of recorded electrodes are illustrated in Supplementary Figure S1. Two additional patch electrodes were positioned at the extraocular canthal positions of both eyes to record electrooculogram (EOG) signals. Electrode impedances were calibrated to be less

than 5 KΩ. Hand movement kinematic data was recorded by the position-detecting sensor fixed on the right hand.

D. Data Preprocessing

The data preprocessing in this study contained two pipelines for EEG signals and kinematic data respectively (see Supplementary Figure S2). All data pre-processing was implemented by MATLAB 2021b (MathWorks, USA) and open source toolbox EEGLAB version 14.1.1 [34].

For the kinematic data, a zero-phase, second-order, low-pass Butterworth filter with a cutoff frequency of 4 Hz was applied. Then, the kinematic data was down-sampled to 10 Hz. The trajectory components (p_x, p_y), distance (p), velocity components (v_x, v_y) and speed (v) were extracted at each sample point. Among which, $p = \sqrt{p_x^2 + p_y^2}$ and $v = \sqrt{v_x^2 + v_y^2}$.

For the EEG signals preprocessing, to avoid signal contamination from peripheral channels and reject the bad channels, we checked each channel and finally selected 30 channels for subsequent analysis, as reflected in Supplementary Figure S1. We selected channels according to the principles of keeping the channels associated with brain regions more related to motor functions while removing channels associated with brain regions less related to motor functions and rejecting the abnormal channels [29], [35]. The human movement information was mainly encoded in central motor regions, and the movement preparation and planning were related to the cognition and perception functions, which were mainly encoded in frontal and parietal regions. Thus, the channels involved in frontal-central-parietal regions were selected. The peripheral channels contained a lot of eye artifacts and movement artifacts, and thus were excluded. Abnormal channels with abnormal signal noise were inspected by eyes and rejected. EEG data was first down- sampled to 100 Hz. A zero-phase, fourth-order, low-pass Butterworth filter with a cutoff frequency of 40 Hz was applied to remove high band artifacts, e.g. muscle artifacts. A sliding-window baseline correction was. used to remove baseline drift. Next, an independent component analysis was performed to remove eye movement artifacts by rejecting the independent components whose correlation coefficients with EOG signals were above 0.4 [36]. Artifact subspace reconstruction (ASR) was then applied to remove movement artifacts arisen from hand movement [37]. In this study, the cutoff parameter of ASR was set to be 30 as recommended in [37]. Next, the common average reference was used to remove spatial noise, and a zero-phase, fourth-order, low-pass Butterworth filter with a cutoff frequency of 2 Hz was used to extract low-frequency information from EEG signals [18] [19]. After that, bad trials with abnormal kurtosis and amplitude exceeding $+/-200\ \mu$V were rejected. Finally, the EEG epochs of [2.5, 4.5] s in each trial, i.e., lasting for 2 s after movement onset, were segmented for further analysis.

E. Decoding Model

The six kinematic movement parameters to be decoded were generated as a response matrix Y, as follows:

$$Y = [p_x, p_y, v_x, v_y, p, v], \quad \in \Re^{(T \cdot N) \times 6}, \tag{2}$$

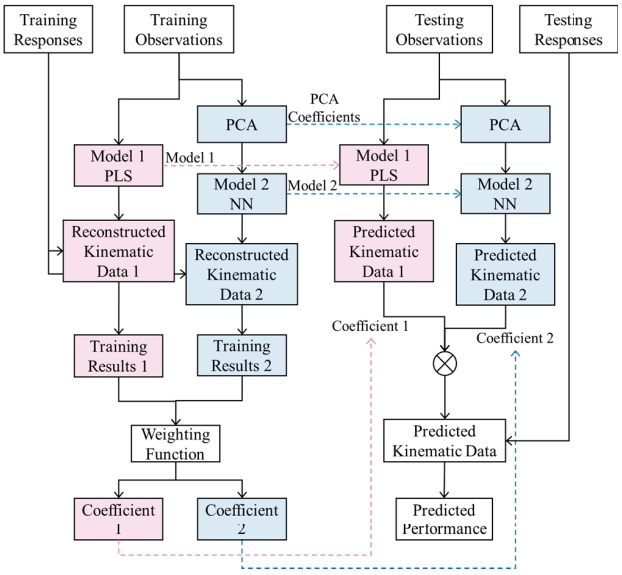

Fig. 3. The flowchart of our proposed adaptive decoder-ensemble framework.

where T is the number of trials, which is 240 for each paradigm, and N is the number of decoded sample points in each trial, which is 20 for a 2-s decoding window with the sampling rate of 10 Hz of the kinematic data. Corresponding to each kinematic data sample, the potential amplitudes of EEG signals from C electrodes and K time lags were first extracted and then re-shaped to a one-dimension vector as one EEG observation, which was used to predict the kinematic information. Time lags referred to the time points before each sample point. In this study, $C = 30$, and $K = 11$, which was with respect to the time lags from -100 ms to 0 ms with a time interval of 10 ms. Thus, an EEG observation matrix X was generated with a shape of $(T \cdot N) \times (C \cdot K)$.

Given a pair of EEG and kinematic datasets, we proposed an adaptive decoder-ensemble framework for the continuous hand movement decoding, as shown in Fig. 3. This framework fused the linear and nonlinear regressors at a decision level. The inspiration of proposing this framework originated from the un-balance of decoding results between trials across decoders. In some trials, the linear regressors could have better decoding performance than the nonlinear regressors, and vice versa. Besides, we found that the kinematic parameter decoding results were usually near zero for the trials with mediocre decoding performance. Thus, we tried to ensemble the decoding results of both linear and nonlinear regressors at the decision level. The predicted results of the two regressors were adaptively combined according to their training performance.

For the linear regressor, we adopted the partial least-squares (PLS) regression, which integrates the multiple linear regression (mLR), principle component analysis (PCA) and canonical correlation analysis, and it is suitable to deal with the predictor variables with strong collinearity. The general multivariate model of PLS could be written as follows:

$$\begin{aligned} X &= W P^T + E \\ Y &= U Q^T + F, \end{aligned} \tag{3}$$

where W is the projection matrix of observation matrix X in the component latent space, U is the projection matrix of response matrix Y in the component latent space, P and Q are the component loading matrixes, E and F are the error terms subject to independent identically distribution. In Equation (3), the matrixes P and Q could be combined into a weight matrix R, and we could reconstruct the kinematic response matrix Y from the observation matrix X in the component latent space by $Y = X \cdot R$. Besides, after our tests, the PLS regression showed better performance on our datasets than other common-used linear regressors, including mLR, least absolute shrinkage and selection operator (LASSO) regression, and ridge regression.

For the non-linear regressor, we applied the neural network (NN) for regression, which could capture the complex relationships between the predictors and responses by numerous neuron units. Specifically, the NN was designed to comprise one Sequential Input layer, one fully connected layer with the neuron size of 200, one ReLU activation layer, and one Output layer. After our tests, the NN outperformed other common-used non-linear regressors on our datasets, including support vector machine regression, random forest regression and Gaussian process regression. Before the NN was used to decode the EEG data, the PCA was applied to reduce the feature dimension into 60.

In the training period, the training results of both the PLS and NN regressors could be obtained. Then, the weighting coefficients of two models, which were used to ensemble the two regressors, were calculated adaptively according to their training performance. The training performance was evaluated by the average Person correlation coefficient (r) between the recorded and the predicted kinematic data across all training trials and six kinematic parameters. The weighting coefficients of two regressors were calculated as follows:

$$c_1 = \frac{r_1}{r_1 + r_2}$$
$$c_2 = \frac{r_2}{r_1 + r_2}, \tag{4}$$

where r_1 is the average r value of the PLS regressor on the training dataset, and r_2 is the average r value of the NN regressor on the training dataset. In the testing period, the predicted kinematic data of two regressors was linearly combined by two weighting coefficients, and the testing performance of the decoder-ensemble model was evaluated by calculating the r value between the recorded and the fused predicted kinematic data across all testing trials.

For each subject, the adaptive decoder-ensemble framework was tested with a 5×5 cross-validation procedure until each fold of the testing data was exhausted. The decoded kinematic data was smoothed with a zero-phase, second-order, low-pass Butterworth filter with a cutoff frequency of 4 Hz. Besides, to estimate the chance level correlation coefficients r_{chance}, we randomly shuffled the response data Y by 100 times to break the association between the observations and the responses. Then, r_{chance} was calculated by applying the same decoding procedure as above.

F. Source Imaging

In order to estimate the brain activation patterns in the source space, we applied the EEG source imaging technique to map the sensor data at cortical level. The source imaging contained two parts: forward modeling of the head model and inverse estimation of the brain sources. The head model was established by importing the ICBM152 boundary element model (BEM) template and co-registering it with the recorded electrodes' positions using the open source software Brainstorm version 11-Nov-2021. The BEM surface was generated by 1922 vertices of scalp, outer skull and inner skull per layer and with the thickness of the layers of 4 mm. The BEM template contained the scalp, skull and brain layers with the conductivities of 1, 0.0125 and 1, respectively. The electrodes' positions were projected onto the scalp. The forward model was estimated based on the OpenMEEG BEM method in the source space of cortex surface. By the forward model, we could obtain the propagation pattern of electrical fields from the cortex layer to the scalp layer. The inverse model was computed by using sLORETA with the normal-to-cortex constrained dipole orientations and minimum norm imaging.

G. Questionnaire

After the experiments, all subjects were required to answer one questionnaire to make an evaluation on the experiments experience. The questionnaire included six questions and was presented in Supplementary Table S1. The aim of this questionnaire was to make one comparison between two experimental paradigms on the task difficulty, physical effort and mental effort.

III. Results and Discussion

A. Behavior Analysis

Fig. 4 shows the behavior analysis results of the hand movement during the experimental periods of [2], [5] s. Fig. 4(a) depicts the grand-average profiles of six kinematic parameters of four movement directions during the experiments of Paradigms 1 and 2, respectively. It could be seen that, for the Paradigm 2, there were obvious amplitude changes of all directional parameters for all four movement directions, while for the Paradigm 1, there were only half of trials who had obvious amplitude changes of directional kinematic parameters along with the X-axis and the remained half of trials had obvious amplitude changes of directional kinematic parameters along with the Y-axis. It demonstrated the effectiveness of Paradigm 2 to make each single trial contribute valid components on both axes, which could eventually contribute to the continuous hand movement decoding performance.

Fig. 4(b) shows the average movement onset time, movement ending time and movement duration time during the experimental movement periods of Paradigms 1 and 2. The movement onset time was detected by finding the first time point whose speed exceeded 0.01 m/s in one trial, and the movement ending time was detected by finding the last time point whose speed exceeded 0.01 m/s in one trial. The movement duration time of one trial was calculating

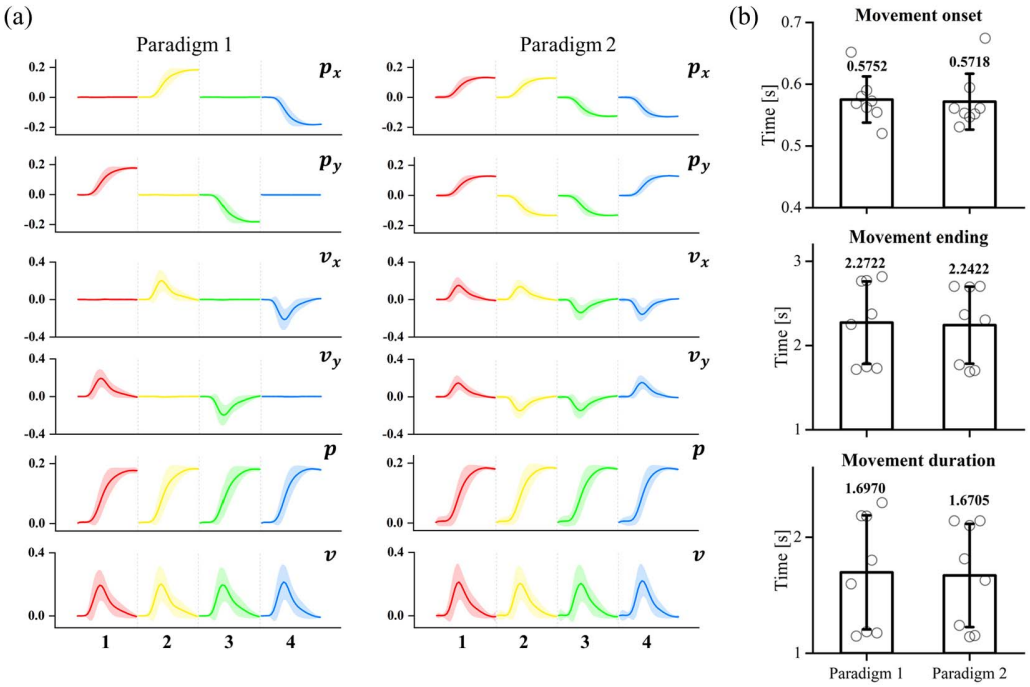

Fig. 4. Behavior analysis results. (a) Grand-average movement parameters profiles for Paradigms 1 and 2, respectively. The red, yellow, green and blue lines correspond to the profiles of hand movement in directions 1, 2, 3, and 4, respectively. The shadow areas are the standard error bands. (b) Grand-average movement onset time, movement ending time and movement duration time for Paradigms 1 and 2, respectively. The bubbles correspond to the average results for each subject.

TABLE I
THE QUESTIONNAIRE RESULTS FOR TWO EXPERIMENTAL PARADIGMS (P. 1 AND P. 2)

Subject No.	Task difficulty		Physical effort		Mental effort	
	P. 1	P. 2	P. 1	P. 2	P. 1	P. 2
S1	3	3	4	3	4	4
S2	4	4	4	3	4	4
S3	3	3	2	2	4	4
S4	3	2	3	3	4	4
S5	3	3	3	2	2	2
S6	3	2	3	2	1	2
S7	1	1	3	2	2	2
S8	3	2	3	2	3	2
Mean± Std	2.9± 0.8	2.5± 0.9	3.1± 0.6	2.4± 0.5	3.0± 1.1	3.0± 1.0

from the ending time minus the onset time. The movement onset time of Paradigms 1 and 2 were 0.5752±0.0374 s and 0.5718±0.0453 s, respectively, the movement ending time of Paradigms 1 and 2 were 2.2722±0.4898 s and 2.2422±0.4577 s, respectively, and the movement duration time of Paradigms 1 and 2 were 1.6970±0.4914 s and 1.6705±0.4446 s, respectively.

The questionnaire results of two experimental paradigms on the task difficulty, physical effort and mental effort are shown in Table I. The average scores of Paradigms 1 and 2 were 2.9± 0.8 and 2.5±0.9 for the task difficulty (Wilcoxon signed-rank test, $p = 0.2500$), respectively, 3.1±0.6 and 2.4±0.5 for the physical effort (Wilcoxon signed-rank test, $p = 0.0312$), respectively, and 2.9±0.8 and 2.5±0.9 for the mental effort (Wilcoxon signed-rank test, $p = 1.0$), respectively. Close scores between two paradigms were obtained for the task difficulty and mental effort, and the significantly lower score of Paradigm 2 was obtained for the physical effort. This could be because the target movement distance in a single trial was 20 cm, which was a little hard for forward and backward movements, and it was easier to move the same distance diagonally. In other words, the single-trial movable range in the 2-D plane increased using the improved center-to-target paradigm.

B. Brain Activity

Fig. 5 shows the grand-average movement-related cortical potentials (MRCPs) at electrode Cz associated with Paradigms1 and 2 across all subjects. The time point 0 s referred to the movement cue time, i.e., the time point 2 s of one trial's timeline (as shown in Fig. 2). It could be seen that, for the MRCPs of both paradigms, the potentials kept stable after 0 s, and there was a slight positive offset at around 0.4 s, followed by a drastic negative offset which peaked negatively at around 0.6 s. After peaking at around 0.6 s, a larger potentials' positive rebound was observed. Note that the negative peak time of both paradigms was almost consistent with the average movement onset time (as shown in Fig. 4). The negative peak amplitudes of Paradigms 1 and 2 were -2.720±1.221 μV and -2.392±1.407 μV, respectively. Wilcoxon signed-rank test showed that there was statistical difference between the

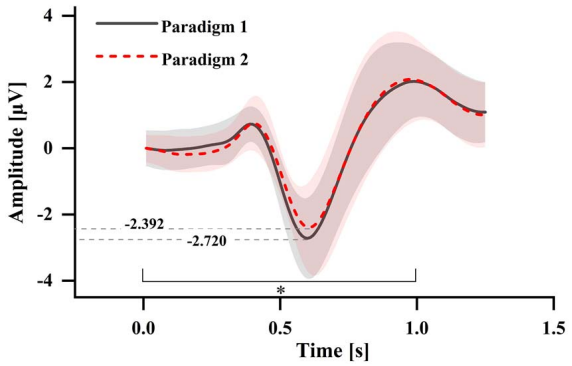

Fig. 5. The grand-averaged MRCPs across all subjects at electrode Cz. Note that time 0 s refers to the movement cue time, i.e., the time point 2 s of one trial's timeline. The shadows of curves represent the standard deviation of the MRCPs across all subjects. The asterisk marks the significant difference between the MRCPs of Paradigms 1 and 2 at epochs [0, 1] s.

MRCPs of Paradigms 1 and 2 in the time periods of [0, 1] s ($p = 0.0391$).

Fig. 6 depicts the grand-average source imaging results in the source space of Paradigms 1 and 2. Time = 0 s corresponded to the movement cue time, i.e., the time point 2 s of one trial's timeline (as shown in Fig. 2). For both Paradigms 1 and 2, similar brain patterns were activated. Before 0.3 s, no obvious brain activity was observed. From the 0.4 s, the patterns of brain activation became apparent with gradually active brain activity and incremental activated brain regions. At the 0.6 s, the brain pattern in the source space was the most active, and the activated cortex covered the primary sensorimotor cortex, supplementary motor cortex, superior parietal lobule cortex, dorsomedial occipital cortex and fronto-central cortex of both hemispheres, in accordance with the findings in [19] and [38]. Besides, the activated brain pattern was mostly centralized in the sensorimotor area, and showed a prominent contralateral distribution. It should be noted that, in this area, we also captured the MRCPs from the low-frequency scalp potentials, as shown in Fig. 5. After the 0.6 s, the state of brain activation declined and tended to be stable with most of energy centralized in the sensorimotor area. To further compare the difference of source patterns between two experimental paradigms, we analyzed the source imaging results obtained by subtracting Paradigm 1 and Paradigm 2. It could be seen that the difference of activation pattern between two paradigms mainly lasted from 0.4 s to 0.8 s and was mainly located at the SM1 area. Besides, the positive brain activity difference indicated that the brain activation during the Paradigm 1 was more active.

The neural coherence between brain activity and behavior could be found. On the one hand, by analyzing the recorded position data, we found that the movement onset time was detected at 0.5752±0.0374 s and 0.5718±0.0453 s for Paradigms 1 and 2, respectively. In the neurophysiological analysis, we observed that the MRCPs peaked negatively at around 0.6 s, and the most active brain pattern was also activated at around 0.6 s. On the other hand, the neural signature results indicated the less physical effort needed for the improved paradigm, which was in accordance with the questionnaire results. As shown in Fig. 5, the average negative peak value of MRCPs was larger in Paradigm 1 (the classic paradigm) than that in Paradigm 2 (the improved paradigm). According to the results in [39], the negative peak value of MRCPs might be related to the torque level, and the negative peak value of MRCPs was larger in the task with the higher torque than in the same task with the lower torque. Similarly, in the source space, when we mapped the activation pattern of Paradigm 1 minus that of Paradigm 2, all activated energy was positive, as shown in Fig. 6. It indicated that brain activity was more active during the experiment of Paradigm 1 than that of Paradigm 2, especially during the movement periods of [0.4, 0.8] s. To sum up, the improved paradigm was less physical effort-demanded for users.

C. Decoding Performance Comparison

One objective of this study was to decode (predict) continuous hand movement kinematic parameter from EEG signals. We quantified the decoding performance by calculating the average Pearson correlation coefficient r between the recorded and decoded kinematic data. Fig. 7 illustrates the decoding performance comparison between different decoding models and two experimental paradigms. Fig. 7(a) compares the correlation coefficient results of using the PLS regressor alone, using the NN regressor alone, and using the decoder-ensemble framework for six decoded kinematic parameters and two paradigms. We applied the two-factor analysis of variance (ANOVA) for the statistical test of decoding results, and the two factors were the decoding models and the decoded parameters. For the Paradigm 1, the two-factor ANOVA showed that there were statistical differences on the decoding results between the decoded parameters ($F(5,125) = 180.34$, $p < 0.001$) and no statistical difference between the decoding models ($F(2,125) = 2.12$, $p = 0.1244$). For the Paradigm 2, the two-factor ANOVA showed that there were statistical differences on the decoding results between the decoded parameters ($F(5,125) = 98.31$, $p < 0.001$) and no statistical difference between the decoding models ($F(2,125) = 2.15$, $p = 0.1211$). From the whole, with using the ensemble framework, the correlation coefficient results were superior to other two models among all six decoded kinematic parameters and both paradigms though it is not significant. The advantage of the ensemble framework lay in that, compared with the common-used models in the existing studies of continuous movement decoding [27], [30], [38], it integrates both the linear and non-linear models for the decoding performance improvement, though it could increase the computation complexity slightly.

Compared with the classic center-out paradigm, in which the hand was required to move in four orthogonal directions along the coordinate axes, the improved center-out paradigm proposed by us, in which the hand was required to move in four orthogonal directions at an angle of 45° from the cartesian coordinate axes, could make the single-trial hand movement have valid projective components on both x and y axes simultaneously. In this case, given the same amount of experimental trials in each direction (in total, there are four directions for both the classic and our paradigms), our

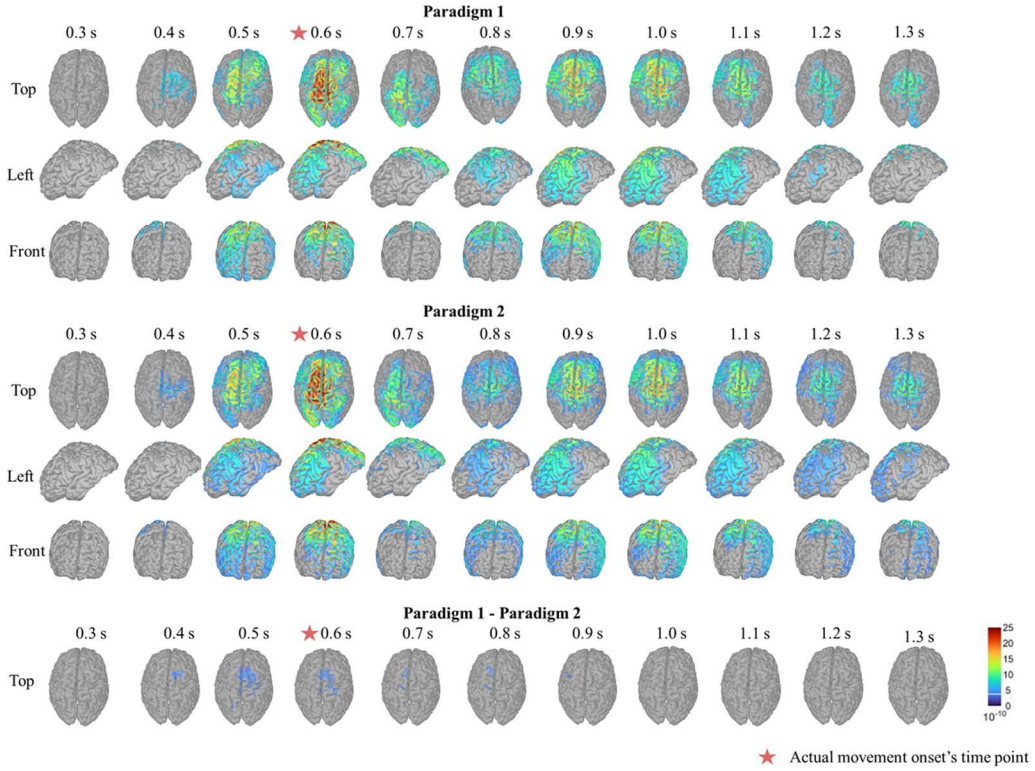

Fig. 6. The grand-averaged activation pattern of two experimental paradigms in the source space. The source imaging results are displayed from time lags 0.3 s to 1.3 s with the time interval of 0.1 s. For each time lag, the source-space activity was imaged from three projection angles: top view, left view, and front view.

paradigm can provide two times amount of training data for building each kinematic parameter decoding model as the classic paradigm. This is because, for the classic paradigm, trials associated with two directions (left and right directions) on the X axis do not generate training data for decoding v_y/p_y. Likewise, trials on the Y axis do not generate training data for decoding v_x/p_x. That is, for a given amount of training data, our paradigm only needs half amount of trials as the classic paradigm. Finally, better continuous decoding performance was obtained based on the improved paradigm.

Fig. 7(b) presents the decoding performance comparison of six kinematic parameters between two paradigms using the adaptive decoder-ensemble framework. Overall, better decoding performance was obtained for the Paradigm 2, especially of the directional kinematic parameters. For p_x, the r values of Paradigms 1 and 2 were 0.14±0.09 and 0.21±0.08, respectively, and Wilcoxon signed-rank test showed the significant statistical difference ($p = 0.0078$). For p_y, the r values of Paradigms 1 and 2 were 0.27±0.09 and 0.38±0.12, respectively, and Wilcoxon signed-rank test showed the significant statistical difference ($p = 0.0156$). For v_x, the r values of Paradigms 1 and 2 were 0.13±0.10 and 0.18±0.10, respectively, and Wilcoxon signed-rank test showed no significant statistical difference ($p = 0.1484$). For v_y, the r values of Paradigms 1 and 2 were 0.21±0.07 and 0.32±0.11, respectively, and Wilcoxon signed-rank test showed the significant statistical difference ($p = 0.0156$). For v, the r values of Paradigms 1 and 2 were 0.58±0.07 and 0.60±0.08, respectively, and Wilcoxon signed-rank test showed no significant statistical difference ($p = 0.3858$). For p, the r values of Paradigms 1 and 2 were 0.69±0.07 and 0.70±0.07, respectively, and Wilcoxon signed-rank test showed no significant statistical difference ($p = 0.5469$). Similar results with the better decoding performance of the paradigm 2 could also be observed when using the PLS or NN models (as reflected in Supplementary Figure S3 and Figure S4). It should be noted that, for the non-directional kinematic parameters, no statistical differences in the decoding performance between the two paradigms were observed. This could be because the non-directional parameters were unrelated to the axis or direction and showed similar profiles of two paradigms, as depicted in Fig. 4.

Furthermore, the chance levels of decoding results were tested by randomly shuffling the testing responses 100 times and testing the proposed model on the shuffled data. Finally, the average r_{chance} values across six kinematic parameters were 0.0071 for Paradigms 1 and 0.0037 for paradigm 2. The decoding results of randomly shuffled kinematic data were significantly lower than those of unshuffled kinematic data (Wilcoxon signed-rank test, $p < 0.001$). This indicated that the adaptive decoder-ensemble model made use of the neural information correlating with hand movement for continuous kinematic parameter decoding instead of decoding by chance.

D. Components Selection

To justify the components number selected for decoding, we compared the decoding performance associated with different number of components using the adaptive decoder-ensemble framework. The number of components ranged

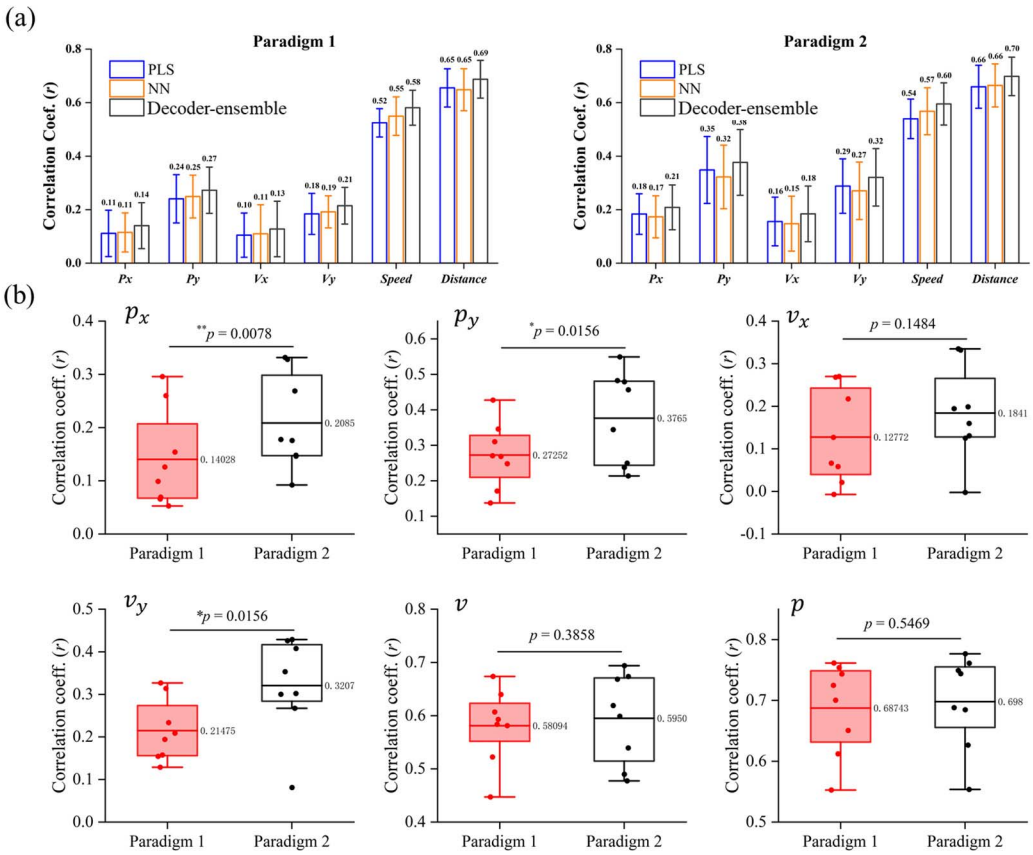

Fig. 7. Decoding performance comparison. (a) The decoding performance comparisons between using the PLS regressor alone, using the NN regressor alone, and using the adaptive decoder-ensemble framework. (b) The decoding performance comparisons of six decoded kinematic parameters between the paradigms 1 and 2. * marks the statistical difference with $p < 0.05$, ** marks the statistical difference with $p < 0.0$.

from 10 to 100, with the increment interval of 10. Specifically, the number of components involved by the PLS and the number of feature dimension reduced by the PCA were the same. Fig. 8 plots the r values curves of different kinematic parameters and two paradigms along with the components number. With the increment of components number, the r values first increased and then kept steady. Relatively higher r values were obtained for the non-directional kinematic parameters p and v. Besides, for each directional kinematic parameter, higher r values were obtained for the paradigm 2 in each components number.

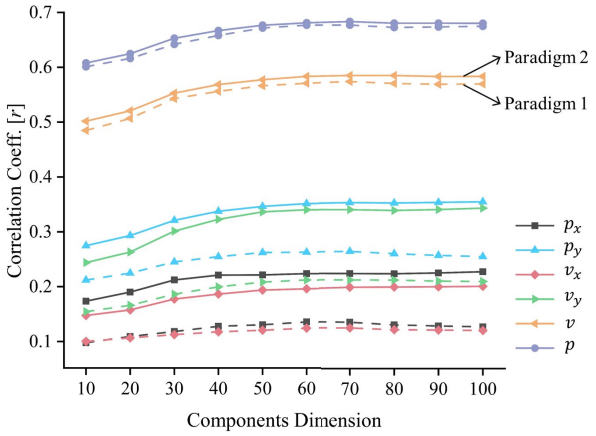

Fig. 8. The r values curves of different kinematic parameters and two paradigms along with the components number. For each parameter, the solid lines correspond to the results of Paradigms 1, and the dotted lines correspond to the results of Paradigms 2.

E. Generalization Performance Test of Two Paradigms

To put the EEG-based continuous hand movement decoding forward into the practical application, realizing the decoding of the users' movement intentions in any arbitrary movement direction, instead of being limited to the pre-defined movement directions, is significant. To test the generalization performance of the classic and improved paradigms in this study, we trained the models using the training data from four movement directions in each paradigm and tested them with the testing data from eight movement directions in both paradigms. It meant that, for both paradigms, we trained their respective models using their respective training data and tested them using the same testing data sets which mixed the testing data from two paradigms. The generalization performance results of two paradigms are shown in Fig. 9. Overall, better generalization performance was obtained using the Paradigms 2. For p_x, the r values of Paradigms 1 and 2 were 0.12±0.08 and 0.15±0.07, respectively, and

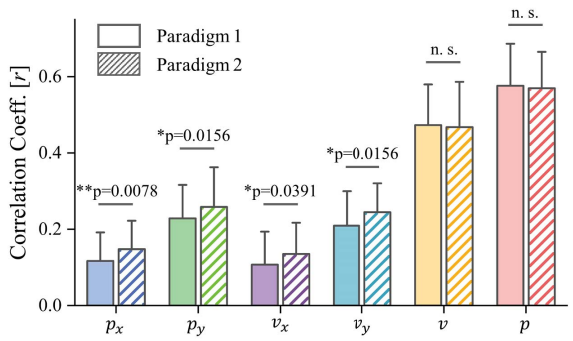

Fig. 9. Generalization performance test results comparisons of two paradigms among six kinematic parameters. Solid bar charts correspond to the results of Paradigms 1, and bar charts with diagonal lines correspond to the results of Paradigms 2. * marks the statistical difference with $p < 0.05$, ** marks the statistical difference with $p < 0.01$, n. s. marks no statistical difference.

Wilcoxon signed-rank test showed the significant statistical difference ($p = 0.0078$). For p_y, the r values of Paradigms 1 and 2 were 0.23±0.09 and 0.26±0.10, respectively, and Wilcoxon signed-rank test showed the significant statistical difference ($p = 0.0156$). For v_x, the r values of Paradigms 1 and 2 were 0.11±0.09 and 0.14±0.08, respectively, and Wilcoxon signed-rank test showed the significant statistical difference ($p = 0.0391$). For v_y, the r values of Paradigms 1 and 2 were 0.21±0.09 and 0.24±0.08, respectively, and Wilcoxon signed-rank test showed the significant statistical difference ($p = 0.0156$). For v, the r values of Paradigms 1 and 2 were 0.47±0.11 and 0.47±0.12, respectively, and Wilcoxon signed-rank test showed no significant statistical difference ($p = 0.7422$). For p, the r values of Paradigms 1 and 2 were 0.58±0.11 and 0.57±0.10, respectively, and Wilcoxon signed-rank test showed no significant statistical difference ($p = 0.6406$). Similar results with the better generalization performance of the Paradigms 2 could also be observed when using the PLS or NN models (as reflected in Supplementary Figure S5 and Figure S6). The significant improved results showed the advantage of extending the single-trial hand movement from the one-dimension motion which was along the coordinate axes to a two-dimensional plane when exploring the continuous hand movement decoding.

F. Discussion of Paradigms Comparison

Common used paradigms for researching the EEG-based continuous hand movement decoding could be divided into three categories: the target-to-target movement task, the pursuit tracking task (PTT), and the self-chosen continuous movement task. In the experiments of PTT, the subjects were asked to control the cursor by hand to track the target on the screen. In this case, it was inevitable that the subjects' eyes would also be tracking the target. Thus, there would be a lot of eye movement artifacts and visual components involved in brain signals. In [19], though eye artifacts were attenuated from the brain signals by using the sparse generalized eye artifact subspace subtraction algorithm and by excluding the EOG and frontotemporal channels, the average r values achieved 0.36 during observed movements (0.49 during executed movements). Thus, the PTT paradigm was not suitable to reveal the intrinsic correlations between the neural activities and hand movement. In the experiments of self-chosen continuous movement task, the subjects were required to move their hands freely and aimlessly. However, in real rehabilitation training and daily assistance scenarios, the movements of patients' hands or upper limbs were usually task-driven or target-driven. For the target-to-target movement paradigm, on the one hand, it did not rely on much eye movements and visual attention. On the other hand, the target-to-target movements could cover most of movement types involved in the rehabilitation and daily life and it had well generalization performance.

IV. Conclusion and Future Work

To overcome the limitations of using the classic center-out paradigm to research EEG-based continuous hand movement decoding, we proposed an improved center-out paradigm and developed an adaptive decoder-ensemble framework to continuously predict hand movement kinematic parameters. As a result, neural coherence was observed between the neural activity and behavior analysis on the movement onset and physical effort. It showed that the improved paradigm had the advantages of less physical effort-demanded. Besides, with the improved paradigm and the ensemble decoding framework, the decoding performance enhanced significantly by about 75 percent for the directional parameters and about 10 percent for non-directional parameters. Furthermore, the generalization performance was improved significantly by about 20 percent for the directional parameters. In summary, these results confirmed that our method could enhance the decoding performance of continuous hand movement, especially its generalization performance, and revealed that the low-frequency EEG signals carried the neural information about the continuous hand movement. Applying the improved EEG paradigm allows us to detect human's continuous movement intention better and promote the application of the EEG-based motor-BCIs for rehabilitation, assistance, and human augmentation.

In future work, we hope to advance the continuous hand movement decoding based on our proposed paradigm into real application scenarios, including improving the decoding performance, testing the decoding model by using the target users, and building real BCI-based systems.

References

[1] J. Wolpaw, N. Birbaumer, D. McFarland, G. Pfurtscheller, and T. Vaughan, "Brain-computer interfaces for communication and control," *Clin. Neurophys.*, vol. 113, no. 6, pp. 767–791, Jun. 2002.

[2] G. Buzsaki, C. A. Anastassiou, and C. Koch, "The origin of extracellular fields and currents–EEG, ECoG, LFP and spikes," *Nature Rev. Neurosci.*, vol. 13, no. 6, pp. 407–420, Jun. 2012.

[3] N. Birbaumer and L. G. Cohen, "Brain-computer interfaces: Communication and restoration of movement in paralysis," *J. Physiol.*, vol. 579, no. 3, pp. 621–636, Mar. 2007.

[4] Y. Liu *et al.*, "Motor-imagery-based teleoperation of a dual-arm robot performing manipulation tasks," *IEEE Trans. Cognit. Develop. Syst.*, vol. 11, no. 3, pp. 414–424, Sep. 2019.

[5] D. Liu *et al.*, "EEG-based lower-limb movement onset decoding: Continuous classification and asynchronous detection," *IEEE Trans. Neural Syst. Rehabil. Eng.*, vol. 26, no. 8, pp. 1626–1635, Aug. 2018.

[6] J. D. R. Millan *et al.*, "Combining brain–computer interfaces and assistive technologies: State-of-the-art and challenges," *Frontiers Neurosci.*, Switzerland, vol. 4, no. 161, pp. 1–15, Sep. 2010.

[7] E. C. Lalor *et al.*, "Steady-state VEP-based brain-computer interface control in an immersive 3D gaming environment," *EURASIP J. Appl. Signal Process.*, vol. 2005, no. 19, pp. 3156–3164, Dec. 2005.

[8] P. Ofner, A. Schwarz, J. Pereira, D. Wyss, R. Wildburger, and G. R. Müller-Putz, "Attempted arm and hand movements can be decoded from low-frequency EEG from persons with spinal cord injury," *Sci. Rep.*, vol. 9, no. 1, pp. 1–15, Dec. 2019.

[9] J. R. Wolpaw and D. J. McFarland, "Control of a two-dimensional movement signal by a noninvasive brain-computer interface in humans," *Proc. Nat. Acad. Sci. USA*, vol. 101, no. 51, pp. 17849–17854, Dec. 2004.

[10] E. W. Sellers, T. M. Vaughan, and J. R. Wolpaw, "A brain-computer interface for long-term independent home use," *Amyotrophic Lateral Sclerosis*, vol. 11, no. 5, pp. 449–455, Oct. 2010.

[11] I.-H. Kim, J.-W. Kim, S. Haufe, and S.-W. Lee, "Detection of braking intention in diverse situations during simulated driving based on EEG feature combination," *J. Neural Eng.*, vol. 12, no. 1, Feb. 2015, Art. no. 016001.

[12] T. Teng, L. Bi, and Y. Liu, "EEG-based detection of driver emergency braking intention for brain-controlled vehicles," *IEEE Trans. Intell. Transp. Syst.*, vol. 19, no. 6, pp. 1766–1773, Jun. 2018.

[13] H. Shibasaki and M. Hallett, "What is the Bereltschaftspotential?" *Clin. Neurophysiol.*, vol. 117, no. 11, pp. 2341–2356, Nov. 2006.

[14] C. Grefkes, S. B. Eickhoff, D. A. Nowak, M. Dafotakis, and G. R. Fink, "Dynamic intra- and interhemispheric interactions during unilateral and bilateral hand movements assessed with fMRI and DCM," *NeuroImage*, vol. 41, no. 4, pp. 1382–1394, Jul. 2008.

[15] C. Gerloff, J. Richard, J. Hadley, A. E. Schulman, M. Honda, and M. Hallett, "Functional coupling and regional activation of human cortical motor areas during simple, internally paced and externally paced finger movements," *Brain*, vol. 121, no. 8, pp. 1513–1531, Aug. 1998.

[16] L. Mercado *et al.*, "Decoding the torque of lower limb joints from EEG recordings of pre-gait movements using a machine learning scheme," *Neurocomputing*, vol. 446, pp. 118–129, Jul. 2021.

[17] N. Robinson, A. P. Vinod, K. K. Ang, K. P. Tee, and C. T. Guan, "EEG-based classification of fast and slow hand movements using wavelet-CSP algorithm," *IEEE Trans. Biomed. Eng.*, vol. 60, no. 8, pp. 2123–2132, Aug. 2013.

[18] R. Sosnik and L. Zheng, "Reconstruction of hand, elbow and shoulder actual and imagined trajectories in 3D space using EEG current source dipoles," *J. Neural Eng.*, vol. 18, no. 5, Oct. 2021, Art. no. 056011.

[19] R. J. Kobler, A. I. Sburlea, V. Mondini, M. Hirata, and G. R. Müller-Putz, "Distance- and speed-informed kinematics decoding improves M/EEG based upper-limb movement decoder accuracy," *J. Neural Eng.*, vol. 17, no. 5, Nov. 2020, Art. no. 056027.

[20] J. Wang, L. Bi, W. Fei, and C. Guan, "Decoding single-hand and both-hand movement directions from noninvasive neural signals," *IEEE Trans. Biomed. Eng.*, vol. 68, no. 6, pp. 1932–1940, Jun. 2021.

[21] A. Schwarz, J. Pereira, R. Kobler, and G. R. Müller-Putz, "Unimanual and bimanual reach-and-grasp actions can be decoded from human EEG," *IEEE Trans. Biomed. Eng.*, vol. 67, no. 6, pp. 1684–1695, Jun. 2020.

[22] M. Jochumsen, I. K. Niazi, D. Taylor, D. Farina, and K. Dremstrup, "Detecting and classifying movement-related cortical potentials associated with hand movements in healthy subjects and stroke patients from single-electrode, single-trial EEG," *J. Neural Eng.*, vol. 12, no. 5, Oct. 2015, Art. no. 056013.

[23] T. Chouhan, N. Robinson, A. P. Vinod, K. K. Ang, and C. Guan, "Wavlet phase-locking based binary classification of hand movement directions from EEG," *J. Neural Eng.*, vol. 15, no. 6, Dec. 2018, Art. no. 066008.

[24] N. Robinson, C. Guan, A. P. Vinod, K. K. Ang, and K. P. Tee, "Multi-class EEG classification of voluntary hand movement directions," *J. Neural Eng.*, vol. 10, no. 5, Oct. 2013, Art. no. 056018.

[25] L. Bi, S. Xia, and W. Fei, "Hierarchical decoding model of upper limb movement intention from EEG signals based on attention state estimation," *IEEE Trans. Neural Syst. Rehabil. Eng.*, vol. 29, pp. 2008–2016, 2021.

[26] W. Fei, L. Bi, J. Wang, S. Xia, X. Fan, and C. Guan, "Effects of cognitive distraction on upper limb movement decoding from EEG signals," *IEEE Trans. Biomed. Eng.*, early access, Jun. 29, 2022, doi: 10.1109/TBME.2022.3187085.

[27] T. J. Bradberry, R. J. Gentili, and J. L. Contreras-Vidal, "Reconstructing three-dimensional hand movements from noninvasive electroencephalographic signals," *J. Neurosci.*, vol. 30, no. 9, pp. 3432–3437, Mar. 2010.

[28] N. Robinson, C. Guan, and A. P. Vinod, "Adaptive estimation of hand movement trajectory in an EEG based brain–computer interface system," *J. Neural Eng.*, vol. 12, no. 6, Dec. 2015, Art. no. 066019.

[29] J.-H. Jeong, K.-H. Shim, D.-J. Kim, and S.-W. Lee, "Brain-controlled robotic arm system based on multi-directional CNN-BiLSTM network using EEG signals," *IEEE Trans. Neural Syst. Rehabil. Eng.*, vol. 28, no. 5, pp. 1226–1238, May 2020.

[30] A. Úbeda, J. M. Azorín, R. Chavarriaga, and J. D. R. Millán, "Classification of upper limb center-out reaching tasks by means of EEG-based continuous decoding techniques," *J. NeuroEngineering Rehabil.*, vol. 14, no. 1, pp. 1–14, Dec. 2017.

[31] J. Lv, Y. Li, and Z. Gu, "Decoding hand movement velocity from electroencephalogram signals during a drawing task," *Biomed. Eng. OnLine*, vol. 9, no. 1, pp. 1–21, Oct. 2010.

[32] J. Cohen, "Statistical power analysis," *Current Directions Psychol. Sci.*, vol. 1, no. 3, pp. 98–101, 1992.

[33] F. Faul, E. Erdfelder, A.-G. Lang, and A. Buchner, "G*Power 3: A flexible statistical power analysis program for the social, behavioral, and biomedical sciences," *Behav. Res. Methods*, vol. 39, no. 2, pp. 175–191, May 2007.

[34] A. Delorme and S. Makeig, "EEGLAB: An open source toolbox for analysis of single-trial EEG dynamics including independent component analysis," *J. Neurosci. Methods*, vol. 134, no. 1, pp. 9–21, Mar. 2004.

[35] M. Jochumsen and I. K. Niazi, "Detection and classification of single-trial movement-related cortical potentials associated with functional lower limb movements," *J. Neural Eng.*, vol. 17, no. 3, Jul. 2020, Art. no. 035009.

[36] J.-H. Kim, F. Biessmann, and S.-W. Lee, "Decoding three-dimensional trajectory of executed and imagined arm movements from electroencephalogram signals," *IEEE Trans. Neural Syst. Rehabil. Eng.*, vol. 23, no. 5, pp. 867–876, Sep. 2015.

[37] C. Chang, S. Hsu, L. Pion-Tonachini, and T. Jung, "Evaluation of artifact subspace reconstruction for automatic artifact components removal in multi-channel EEG recordings," *IEEE Trans. Biomed. Eng.*, vol. 67, no. 4, pp. 1114–1121, Apr. 2020.

[38] R. J. Kobler, A. I. Sburlea, and G. R. Müller-Putz, "Tuning characteristics of low-frequency EEG to positions and velocities in visuomotor and oculomotor tracking tasks," *Sci. Rep.*, vol. 8, no. 1, Dec. 2018, Art. no. 17713.

[39] Y. Gu, F. D. Nascimento, M.-F. Lucas, and D. Farina, "Identification of task parameters from movement-related cortical potentials," *Med. Biol. Eng. Comput. volume*, vol. 47, no. 12, pp. 1257–1264, Dec. 2009.